Journal of Multidisciplinary Engineering Science and Technology (JMEST)
ISSN: 2458-9403
Vol. 9 Issue 3, March - 2022

Toward A Full-Cycle-Growth Model Of A Fission Yeast Cell Using The Finite Element Method

Najib A. Kasti
ATTAWAKOL Company
Beirut, Lebanon
e-mail: najib01@idm.net.lb

***Abstract*—Building on our previous publications, this paper develops further the full-cycle-growth model of a fission yeast cell. The paper is divided into two main parts.**
The first part models the pressurization of the New End (NE) as the primary septum is fully digested. At this stage, the secondary septum/NE thickness is taken to be half the wall thickness. However, it is assumed that while the Old End (OE) is growing, the wall material of the NE will build up so that the thickness of the NE becomes twice its current value. Subsequently, both ends will continue to grow till the new septum wall is formed again.
The second part deals with the growth of both ends, which is based on a growth function that was derived previously from the self-similarity growth principle. The spatial distribution of this growth function was mainly limited to the OE/NE.
Numerically, the growth of the cell was modeled using the finite element method. Since growth almost doubles the cell length, and is mostly restricted to the top/bottom of the cell, the original mesh needs to be updated as growth progresses. This was accomplished by an element division scheme as described in the paper.

Keywords—fission yeast cell; New End pressurization; full- cycle-growth model; finite element method.

Table of Content

I. Introduction

The full-cycle growth of a fission yeast cell involves five main processes [1-9], as summarized in Fig. 1 [1,2].

a. The digestion of the primary septum wall and the division of the cell.
b. The NE pressurization.
c. Growth of the OE.
d. The delayed growth of the NE.
e. The formation of new septum wall.

These processes occur under high turgor pressure, which may exceed 1 MPa.

The previous publications [1,2] dealt with determining the growth function α.Φ(s) for part (c), which was based on the principle of self-similarity of growth. This growth function related the rate of viscous strain to the elastic strain through the relation

$$d\boldsymbol{\varepsilon}^v/dt = \alpha.\Phi(s).\boldsymbol{\varepsilon}^e \qquad (1)$$

where α is a growth factor, Φ(s) is the growth function that depends on the meridional distance, s, the arc length measured from the tip of the OE/NE. The value of $\Phi(s)|_{s=0}$ is 1.

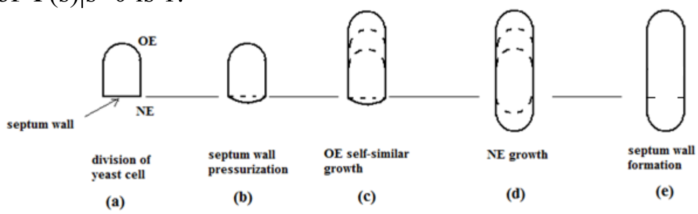

Fig. 1. Fission yeast cell growth cycle [1,2]

Building on our previous work, we further develop in this paper the full-cycle-growth model of a fission yeast cell. The paper is divided into two main parts.
The first part models the pressurization of the New End (NE) as the primary septum is fully digested. At this stage, the secondary septum/NE thickness is taken to be half the wall thickness. However, it is assumed that while the Old End (OE) is growing, the wall material of the NE will build up so that the thickness of the NE becomes twice its current value. Afterwards, both ends will continue to grow till the new septum wall is formed again.
The second part deals with the growth of both ends, which is based on a growth function that was derived previously from the self-similarity growth principle.

The spatial distribution of this growth function was mainly limited to the OE/NE.
Numerically, the growth of the cell was modeled using the finite element method. Since growth almost doubles the cell length, and is mostly restricted to the top/bottom of the cell, the original mesh needs to be updated as growth progresses. This was accomplished by an element division scheme as described in the paper.

II. New End Pressurization - Nonlinear Elastic Analysis – Total Lagrangian formulation

In formulating the problem of NE pressurization the Total Lagrangian method [10-12] was used.
The cell was assumed to be axisymmetric and the deformation as well.
The motion of the body could be represented graphically as shown in figure 2, below.

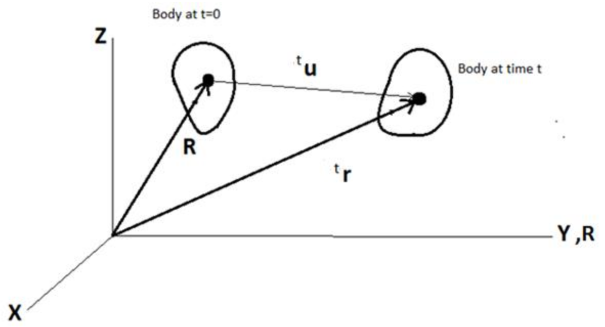

Fig.2 Motion of the axisymmetric body

The formulation of body motion was based on a general curvilinear coordinate system (CS), which was later restricted to the cylindrical CS.
The curvilinear coordinates, in this case, are:

$$\mathbf{\Theta} = (\Theta^1, \Theta^2, \Theta^3) = (R, Z, \theta) \qquad (2)$$

For the undeformed configuration, which corresponds to time “0”, the position vector **R** could be expressed as

$$\mathbf{R} = R.\cos(\theta).\mathbf{I} + R.\sin(\theta).\mathbf{J} + Z.\mathbf{K} = R.\mathbf{e}_R + Z.\mathbf{e}_Z \qquad (3)$$

where

$$\mathbf{e}_R(\theta) = \cos(\theta).\mathbf{I} + \sin(\theta).\mathbf{J}\ ,\ e_Z = \mathbf{K}\text{ , and}$$
$$\mathbf{e}_\theta(\theta) = -\sin(\theta).\mathbf{I} + \cos(\theta).\mathbf{J} \qquad (4)$$

The corresponding covariant base vectors are given by:

$$^o\mathbf{g}_1 = \partial\mathbf{R}/\partial\Theta^1 = \partial\mathbf{R}/\partial R = \cos(\theta).\mathbf{I} + \sin(\theta).\mathbf{J} = \mathbf{e}_R \qquad (5)$$
$$^o\mathbf{g}_2 = \partial\mathbf{R}/\partial\Theta^2 = \partial\mathbf{R}/\partial Z = \mathbf{K} = \mathbf{e}_Z$$
$$^o\mathbf{g}_3 = \partial\mathbf{R}/\partial\Theta^3 = \partial\mathbf{R}/\partial\theta = -R.\sin(\theta).\mathbf{I} + R.\cos(\theta).\mathbf{J} = R.\mathbf{e}_\theta$$

The metric tensor for the undeformed convected system is given by:

$$^o g_{ij} = {^o\mathbf{g}_i} \cdot {^o\mathbf{g}_j} \qquad (6)$$

The determinant of $^o g_{ij}$ is

$$^o g = \det[^o g_{ij}] \qquad (7)$$

and, in the case of a cylindrical CS,

$$^o g = R^2 \qquad (8)$$

The contravariant base vectors satisfy the relation: $^o\mathbf{g}^A \cdot {^o\mathbf{g}_B} = \delta^A_B$, which leads to:

$$^o\mathbf{g}^1 = e_R\ ;\ \ ^o\mathbf{g}^2 = e_Z\ ;\ \ ^o\mathbf{g}^3 = (1/R).e_\theta \qquad (9)$$

The strains, stresses and stress-strain relations are as follows:

a. <u>Convariant Components of Strains</u>

The strains at time t could be expressed as:

$$^t_o\boldsymbol{\Upsilon} = {^t_o\Upsilon_{AB}} \cdot {^o\mathbf{g}^A} \otimes {^o\mathbf{g}^B} \qquad (10)$$

where the symbol ⊗ represents the tensor product.

The physical components of the strain are written as $<{^t_o\Upsilon_{AB}}>$ with their values determined by the following equation:

$$<{^t_o\Upsilon_{AB}}> = {^t_o\Upsilon_{AB}} \cdot ||{^o\mathbf{g}^A}|| \cdot ||{^o\mathbf{g}^B}|| \qquad (11)$$

where $||{^o\mathbf{g}^A}||$ is the norm of the contravariant base vector.

b. “ <u>Second Piola-Kirchhoff” Stress Tensor</u>

A “ first Piola-Kirchhoff” stress tensor could be expressed as

$$^t_o\mathbf{P} = {^t_o P^{Ab}} \cdot {^o\mathbf{g}_A} \otimes {^t\mathbf{g}_b} \qquad (12)$$

and a “ second Piola-Kirchhoff” stress tensor could be defined by the following relation:

$$^t_o\mathbf{S} = \{ {^t_o P^{Ab}} \cdot {^o\mathbf{g}_A} \otimes {^t\mathbf{g}_b} \} \cdot \{ {^t\mathbf{g}^c} \otimes {^o\mathbf{g}_C} \} = {^t_o P^{Ab}} \cdot {^o\mathbf{g}_A} \otimes {^o\mathbf{g}_B}$$
$$= {^t_o S^{AB}} \cdot {^o\mathbf{g}_A} \otimes {^o\mathbf{g}_B} \qquad (13)$$
$$\Rightarrow\quad {^t_o S^{AB}} = {^t_o P^{Ab}}$$

The physical components of the stress tensor are written as $<{^t_o S^{AB}}>$ with values determined by the following equation:

$$<{^t_o S^{AB}}> = {^t_o S^{AB}} \cdot ||{^o\mathbf{g}_A}|| \cdot ||{^o\mathbf{g}_B}|| \qquad (14)$$

where $||{^o\mathbf{g}_A}||$ is the norm of the covariant base vector.

b. The <u>stress-strain relation</u> is assumed to be the isotropic Saint-Venant-Kirchhoff model between physical components (which has its own limitations [10])

$$<{^t_o S^{AB}}> = [E/(1+\nu)]^* <{^t_o\Upsilon_{AB}}> - [\nu^* E/(1-2\nu)]^* <{^t_o\Upsilon_{CC}}>^* \delta^{AB} \qquad (15)$$

with

E = Elastic modulus
v = Poisson's ratio

c. Applying the method of weighted residual to the equation of motion leads to (with neither body forces nor acceleration)

$$\{ \int_{ov} [{}^t_oP^{Ab}(\mathbf{\Theta}) \,.\, {}^t\mathbf{g}_b(\mathbf{\Theta}) \,.\, \partial/\partial(\Theta^a) [\, \mathbf{w} \,] \,] \} d^ov = \{ \int_{oa} [{}^t_o\mathbf{T}(\mathbf{\Theta}) .\, \mathbf{w} \,] \} d^oa \quad (16)$$

where $\mathbf{w}$ is the weight function and ${}^t_o\mathbf{T}(\mathbf{\Theta})$ is the traction vector (= $d^t_o\mathbf{F}/d^oa$ where ${}^t_o\mathbf{F}$ is the applied load at time "t" and ^oa is the original surface area).

d. Finite Element Discretization

By discretizing the domain, the weight function is expressed as

$\mathbf{w} = w^\alpha(\mathbf{\Theta}) \,.\, \mathbf{e}_\alpha = \phi_N(\mathbf{\Theta}) \,.\, w^{N\alpha} \,.\, \mathbf{e}_\alpha$, α = 1,2 (=R,Z)

where

ϕ_N= the shape function of node "N" and $\mathbf{\Theta} = [{}^or, {}^oz] = [R,Z]$ (17)

Since $w^{N\alpha}$ is arbitrary, we get

$$\int_{ov} \partial/\partial(\Theta^a) [\phi_N(\mathbf{\Theta}).\mathbf{e}_\alpha] \,.\, {}^t_oP^{Ab}(\mathbf{\Theta}) \,.\, {}^t\mathbf{g}_b(\mathbf{\Theta})] d^ov = \int_{oa} \phi_N(\mathbf{\Theta}) \,.\, [{}^t_o\mathbf{T}(\mathbf{\Theta}).\, \mathbf{e}_\alpha \,] \, d^oa \quad (18)$$

The above equation could be written in matrix form as:

$$\int_{ov} (\mathbf{B})^T \,.\, {}^t_o\mathbf{P} \,.\, d^ov = {}^t_oF(p, {}^t\mathbf{u}) \quad \text{or} \quad \mathbf{K}({}^t\mathbf{u}) = \mathbf{F}({}^tp, {}^t\mathbf{u}) \quad (19)$$

where

${}^t_o\mathbf{P} = [{}^t_oP^{11} \; {}^t_oP^{22} \; {}^t_oP^{33} \; {}^t_oP^{12}]^T$, ${}^tp$= pressure , and ${}^t\mathbf{u}$ = deformation (20)

e. Linearization of Linear Momentum Equation: $\mathbf{K}({}^t\mathbf{u})=\mathbf{F}({}^tp, {}^t\mathbf{u})$

For the static analysis, the residual $\mathbf{R}_N$ is expressed as:

$$\mathbf{R}_N = \int_{ov} \{ \mathbf{B}_N{}^T \,.\, {}^t_o\mathbf{P} \} d^ov - {}^t_o\mathbf{F}_N = 0 \quad (21)$$

Linearization about $\mathbf{u}_*$ leads to:

$$\int_{ov} \{\Sigma_L\{ [(\partial\mathbf{B}_N{}^T/\partial^t{}_o\mathbf{u}^L)] \,.\, {}^t_o\mathbf{P} + \mathbf{B}_N{}^T.[(\partial^t_o\mathbf{P}/\partial^t{}_o\mathbf{u}^L)\} d^ov \}|_*.\Delta({}^t{}_o\mathbf{u}^L) - \Sigma_L [(\partial\mathbf{F}_N/\partial^t{}_o\mathbf{u}^L)] \,|_*.\Delta({}^t{}_o\mathbf{u}^L) = -\int_{ov}\{ \mathbf{B}_N{}^T.{}^t_o\mathbf{P} \} d^ov|_* + {}^t_o\mathbf{F}_N |_* \quad (22)$$

f. The applied load vector is expressed as:

$${}^t_oF_{N\alpha} = \int_{oa} {}^tp \,.\, {}^on_A \,.\, [{}^tg/{}^og]^{(1/2)} \,.\phi_N(R,Z).[{}^t\mathbf{g}^a \,.\, \mathbf{e}_\alpha] d^oa \quad (23)$$

where
${}^tp$ = pressure at time "t"
${}^on_A$ = normal vector in the undeformed configuration
${}^og$ = determinant of metric tensor at time "0"
${}^tg$ = determinant of metric tensor at time "t"
$\phi_N(R,Z)$ = shape function of node "N"
${}^t\mathbf{g}^a$ = contravariant base vector at time "t" in direction "a"
$\mathbf{e}_\alpha$ = unit vector in direction "α"
d^oa = original differential area

Fig. 3 shows the pressurization of a flat NE into a curved end due to a pressure of 1.5 MPa.

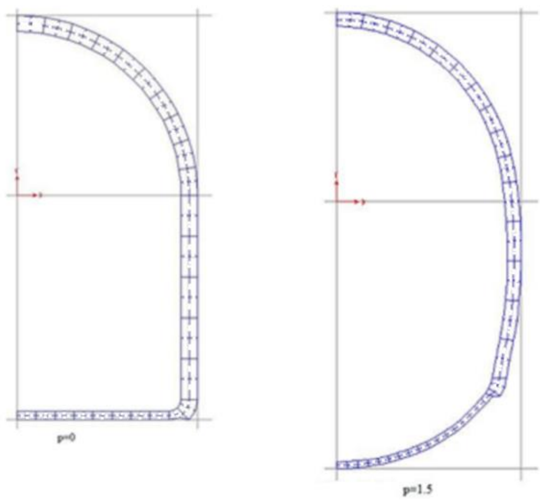

Fig. 3 Pressurization of NE with a pressure of p=1.5 MPa

III. Viscous Growth of Cell

After the division of the cell and pressurization of the New End the OE starts to grow, followed by the growth of the NE (by about an hour) [5].

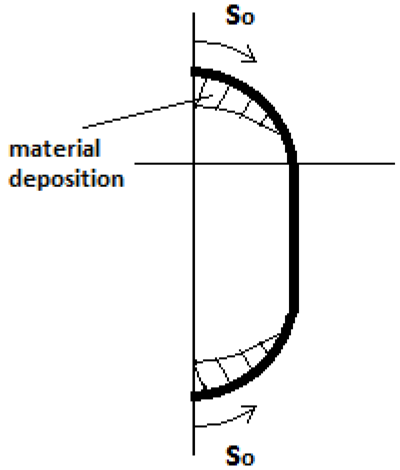

Fig. 4 Material deposition along ends of cell

Journal of Multidisciplinary Engineering Science and Technology (JMEST)
ISSN: 2458-9403
Vol. 9 Issue 3, March - 2022

The growth of the cell is the result of material deposition that diffuses into the cell wall and leads to the breakage of bonds, as shown in fig. 4. This in turn reduces the stiffness of the wall and increases its viscous flow.

Mathematically, this process was expressed by a rate function of viscous strain [1,2]

$$d\boldsymbol{\varepsilon}^v/dt=\alpha.\Phi(s).\boldsymbol{\varepsilon}^e \quad (24)$$

where α is a growth factor, Φ(s) a growth function that depends on the meridional distance "s", the arc length measured from the tip of the OE/NE. The value of $\Phi(s)|s=0$ is 1.

In modeling the growth of a fission yeast cell three configurations were used, as shown in Fig. 5 [1,2] :
a) The plasmolysed configuration "0".
b) The elastically deformed cell configuration by turgor pressure "1".
c) The configuration where material deposition and growth occur within the cell under turgor pressure"2".
The plasmolysed configuration "0" when subjected to turgor pressure expands to configuration "1" with large elastic deformations. Material deposition, which softens the cell wall, leads to configuration "2" when coupled with the turgor pressure.

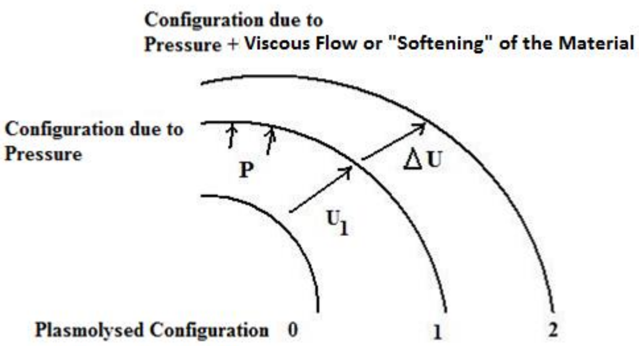

Fig. 5 The three configurations of growth of a fission yeast cell [1,2]

Modeling the viscous growth of the "spherical" parts of the fission yeast cell follows the steps described below for an interval of time $[t_1,t_2]$:

a. The plasmolysed configuration was pressurized and the elastic strains $\boldsymbol{\varepsilon}^e(R,Z)$ were computed at the Gauss points (gp) using the finite element method.

$$\boldsymbol{\varepsilon}^e(R_{gp},Z_{gp}) = \mathbf{B}(R_{gp},Z_{gp}).\mathbf{u} \quad (25)$$

where

$\mathbf{B}(R_{gp},Z_{gp})$ = strain matrix (gradient of shape functions) at the Gauss points, **u** = nodal deformations

b. The increase in the viscous strain is calculated at the Gauss points of part "a" as follows:
- Calculate the arc-length (s) of the Gauss point starting from the tip.
- Compute α.Φ(s) as in the previous publications [1,2].
- Calculate the viscous strain increment of a Gauss point,

$$\Delta\boldsymbol{\varepsilon}^v(R_{gp},Z_{gp}) = \alpha.\Phi(s).\ \boldsymbol{\varepsilon}^e(R_{gp},Z_{gp}).\ \Delta t \quad (26)$$

- Determine the nodal loads due to viscous strains, $\mathbf{F}^v$:

$$\mathbf{F}^v = \int \mathbf{B}^T.\ D.\ \Delta\boldsymbol{\varepsilon}^v\ .dV \quad (27)$$

where
D = elastic constitutive matrix

- Solve for the viscous deformations using

$$\mathbf{K}_T\ .\ \Delta\mathbf{u}^v = \mathbf{F}^v \quad (28)$$

IV. Growth and Mesh Update

The simulation of growth in the interval $[t_1,t_2]$ of the previous section is repeated until full growth is achieved.
At the end of each interval $[t_1,t_2]$, the ratio of length(L)/width(w) of each element is checked:

a. If L/W < ratio_allowed , the mesh is not modified.
b. If L/W > ratio_allowed, the element is split into two elements.

It is assumed that the material properties (E,ν) return to original values after each interval of growth. Consequently, there is no issue with specifying the new material property for each new element.
The element used was a 9-node axisymmetric element. It was divided as follows:

i- Specify new six nodes, three on the middle left and three on the middle right of each element to be divided.
ii- Divide the element in question into two, with the middle nodes becoming the new boundaries.

The resulting mesh is shown in Fig. 6, below.

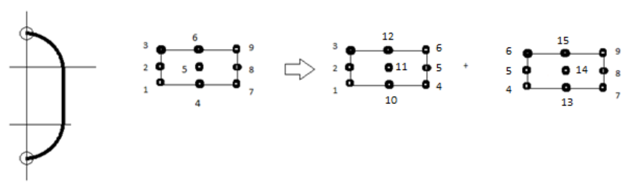

Fig. 6 Division of elements

When the above growth process is applied to the fission yeast cell, the growth of the OE after the first 24 minutes, and the division of the top element into two, are shown in Fig. 7.

Since the speed of growth is around 2μm/hr, for 24 minutes the growth is $\Delta \sim 2\mu m/hr*(24/60) = 0.8\ \mu m$. The viscous growth computed from the finite element solution was around 0.84 μm.

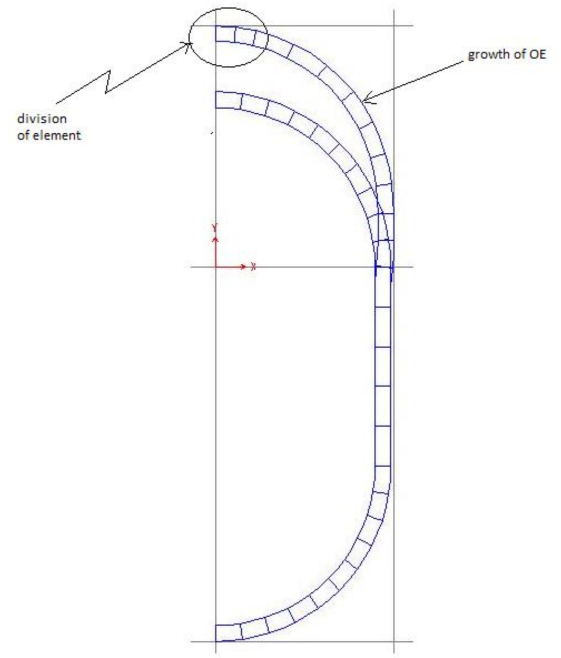

Fig. 7 Growth of OE and division of top element

V. CONCLUSIONS

This paper modeled two processes from the full-cycle-growth model of a fission yeast cell.

The first process was the pressurization of New End, which involves large elastic deformations. The Total Lagrangian formulation, based on the cylindrical convected coordinate system, was used for this purpose.

The second process involved modeling the growth of the Old End/New End due to viscous flow. The rate of the viscous strains was assumed to be proportional to the elastic strain by a factor representing the growth function. Since growth occurs mostly at the ends, with a doubling in cell length, updating the mesh was deemed necessary. This is needed to prevent excessive element distortion and to better capture the viscous strain distribution at both ends. The mesh was updated through element division as growth progressed.

REFERENCES

[1]. Kasti, N., “Modeling the Growth of a Fission Yeast Cell Using the Self-Similarity Growth Principle - A Simplified Approach”, Journal of Multidisciplinary Engineering Science and Technology, vol. 6, Issue 3, 2019.

[2]. Kasti, N., “A Numerical Integration Scheme for the Growth of a Fission Yeast Cell Based on the Self-Similarity Growth Principle”, Journal of Scientific and Engineering Research, 6(5): 89-94, 2019.

[3] J. Abenza et al., “Wall mechanics and exocytosis define the shape of growth domains in fission yeast,” Nature Communications,6:8400, doi: 10.1038/ncomms9400, 2015.

[4] T. Drake and D. Vavylonis, “Model of fission yeast cell shape driven by membrane-bound growth factors and the cytoskeleton,” PLOS Computational Biology, Vol. 9, Issue 10, 2013.

[5] J. Mitchison and P. Nurse “Growth in cell length in the fission yeast Schizosaccharomyces Pombe,” J. Cell Sci., 75, pp. 357-376, 1985.

[6] R. Bernal, E. Rojas and J. Dumais, “The mechanics of tip growth morphogenesis: what we have learned from rubber ballons,” Journal of Mechanics of Materials and Structures, Vol. 2, No. 6, 2007.

[7] E. Atilgan, V. Magidson, A. Khodjakov and F. Chang, “Morphogenesis of the fission yeast cell through cell wall expansion,” Current Biology, 25(16), pp. 2150-2157, 2015.

[8] O. Campas and L. Mahadevan, “Shape and dynamics of tip-growing cells,” Current Biology, 19, pp. 2102-2107, 2009.

[9] O. Goriely and M. Tabor, “Self-similar tip growth in filamentary organisms,” The American Physical Society, Physical Review Letters, Vol. 90, No. 10, 2003.

[10] K. Hjelmstad, Fundamentals of Structural Mechanics, 2nd edition, Springer, 2005.

[11] J. T. Oden, Finite Elements of Nonlinear Continua, McGraw-Hill, 1972.

[12] J. T. Oden, and J. E. Key, “Numerical Analysis of Finite Axisymmetric Deformations of Incompressible Elastic Solids of Revolution”, Int. J. Solid Structures, Vol. 6, pp 497-518, 1970.